Graph Attention Networks for Channel Estimation in RIS-assisted Satellite IoT Communications

Kürşat Tekbıyık, *Graduate Student Member, IEEE*, Güneş Karabulut Kurt, *Senior Member, IEEE*,
Ali Rıza Ekti, *Senior Member, IEEE*, Halim Yanikomeroglu, *Fellow, IEEE*

Abstract—Direct-to-satellite (DtS) communication has gained importance recently to support globally connected Internet of things (IoT) networks. However, relatively long distances of densely deployed satellite networks around the Earth cause a high path loss. In addition, since high complexity operations such as beamforming, tracking and equalization have to be performed in IoT devices partially, both the hardware complexity and the need for high-capacity batteries of IoT devices increase. The reconfigurable intelligent surfaces (RISs) have the potential to increase the energy-efficiency and to perform complex signal processing over the transmission environment instead of IoT devices. But, RISs need the information of the cascaded channel in order to change the phase of the incident signal. This study proposes graph attention networks (GATs) for the challenging channel estimation problem and examines the performance of DtS IoT networks for different RIS configurations under GAT channel estimation. It is shown that the proposed GAT both demonstrates a higher performance with increased robustness under changing conditions and has lower computational complexity compared to conventional deep learning methods. Moreover, bit error rate performance is investigated for RIS designs with discrete and non-uniform phase shifts under channel estimation based on the proposed method. One of the findings in this study is that the channel models of the operating environment and the performance of the channel estimation method must be considered during RIS design to exploit performance improvement as far as possible.

Index Terms—IoT networks, LEO satellites, non-ideal reconfigurable intelligent surfaces, graph attention networks.

I. INTRODUCTION

Internet of things (IoT) networks are expected to grow with approximately 20% in terms of compound annual growth [1]. In other words, more than 100 billion devices will be connected in massive ubiquitous networks [2, 3]. This growth brings a backhauling gap for the ubiquitously connected massive number of IoT devices. In this context, dense low-Earth orbit (LEO) satellite deployments can be an enabler for global service of IoT devices. Low-power LEO satellites have been already in service [4]. However, a new paradigm, which is called as direct-to-satellite (DtS), has been recently emerged to connect IoT devices directly to satellites without any gateways on the ground [5].

K. Tekbıyık is with the Department of Electronics and Communications Engineering, İstanbul Technical University, İstanbul, Turkey, e-mail: tekbiyik@itu.edu.tr

G. Karabulut Kurt is with the Department of Electrical Engineering, Polytechnique Montréal, Montréal, Canada, e-mail: gunes.kurt@polymtl.ca

A. R. Ekti is with the Grid Communications and Security Group, Oak Ridge National Laboratory, Oak Ridge, TN, U.S.A., e-mail: ektia@ornl.gov

H. Yanikomeroglu is with the Department of Systems and Computer Engineering, Carleton University, Ottawa, Canada, e-mail: halim@sce.carleton.ca

Even though geostationary orbit (GEO) satellites have been proposed for narrowband-IoT applications [6, 7], high delay and high path loss caused by the distance of GEO satellites to the Earth reduce the energy-efficiency. On the other hand, LEO satellite constellations become a prominent way to support global IoT network with a reasonable path delays [8, 9]. Furthermore, the required transmit power for LEO orbits is lower due to the relatively short distance to Earth. For LEO satellite assisted IoT communications, two methods are employed: indirect link and direct (i.e., DtS) transmission links. Direct access is preferred due to the following reasons: the cost of the gateway infrastructure, temporary device deployments for specific environments, and operation ability after any disaster [4]. However, DtS requires a steerable antenna at ground stations (i.e., IoT devices) for tracking owing to the motion of LEO satellites. Furthermore, a sophisticated transceiver is needed in IoT devices to recover the received signal. Considering the hardware limitation and battery capacity for IoT devices, these requirements cannot be met. Rather than an advanced transceiver in each IoT device, it is possible to apply complex signal processing methods over the propagation medium [10].

Smart artificial surfaces, referred to as reconfigurable intelligent surface (RIS), have been recently proposed to shift the processes on the receiver to propagation medium by adjusting the incident wave phase [11]. In other words, coding or complex processing is not needed by RISs. The most appealing feature of RISs is to comprise only passive elements with a single RF chain [12]. Thus, RISs fit well to LEO satellites considering their size, weight, and power (SWaP) constraints [13]. The recent prototypes [14–16] demonstrate that it is possible to decrease the size and weight of the transceiver compared to the conventional multiple-input multiple-output (MIMO) systems. Moreover, the battery life of IoT devices is extended because of decreasing processing energy [17]. It should be highlighted that RISs can be a game-changer for DtS IoT systems since RISs reduce both the required transmit power and hardware complexity. Furthermore, our previous works [13, 18] present that RISs can improve the system performance for LEO inter-satellite links and achieved data rate for satellite-IoT systems, respectively. It is demonstrated that utilizing RISs in DtS system provides two-fold advantages. By focusing the beam towards the receiver, signal-to-noise ratio (SNR) can be maximized while remaining the transmit power same. The second advantage is the decrease in computational complexity of transceiver by processing the transmitted signal on the propagation medium rather than the receiver.

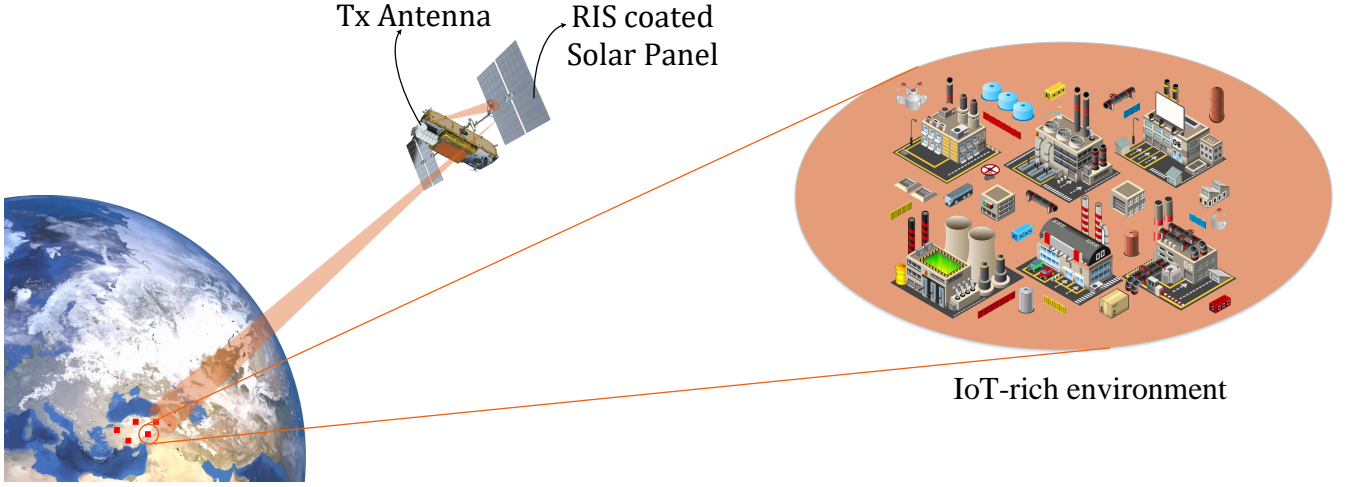The current literature clearly shows that RISs can pro-

Fig. 1. It is possible to enhance the QoS for satellite-IoT systems by utilizing RIS. Therefore, the required power can be reduced for the same data rate and error probability.

vide many attractive features for DtS IoT systems. A few of these are the energy-efficiency, improved achievable rate, beamforming, and tracking. However, in order to take advantage of all these attractive features, channel state information (CSI) must be obtained properly. The main challenge in channel estimation for RIS-assisted communications is that the received signal includes cascaded channel coefficients. To cope with the channel estimation problem, some methods have been proposed. The first methodology [19, 20] utilizes a conventional view for channel estimation by activating a single RIS element for each time instance during the training phase. In other words, the channel coefficients are individually estimated by switching RIS elements on and off. Considering the switching time and total pilot overhead, it can be concluded that this method cannot be efficiently employed on RIS-assisted DtS system because of the longer training signal than channel coherence time [21]. Concisely, acquired channel coefficients regarding RIS elements by this method are not time-invariant. It is known that RISs comprise only passive reflecting/scattering elements; hence, they cannot acquire CSI by themselves. A recent approach in [22] designs RIS in which some elements are active to estimate channel coefficients at RISs. Please note that increasing the number of active elements on RIS means that problems related to SWaP constraints will probably arise. Therefore, this method is not desired for satellite systems.

To address the challenges related to the channel estimation in RIS-assisted wireless communications, we have recently proposed a channel estimator based on graph attention network (GAT) [23]. It should be noted that to the best knowledge of the authors, there is no channel estimation method based on graph neural networks except our recent work on the GAT channel estimator, yet. The motivation behind using GATs for channel estimation can be listed as (i) they can estimate all channel coefficients without an on-off switch mechanism, (ii) their computational complexity is relatively low [24], (iii) they can be generalized over unobserved graphs due to the attention mechanism [25]. Briefly, the GAT channel estimator

can reduce lower pilot overhead as it requires a single pilot signaling subframe to estimate channel coefficients regarding all RIS elements. Furthermore, GAT estimator can continue to perform well under variable channel conditions, thanks to the attention mechanism [23].

Moreover, this study investigates bit error rate (BER) performance of the DtS systems under more practical RIS designs unlike the prior works [13, 26, 27] on wireless communications assisted by hypothetical RISs with continuous phase shift capability. While hypothetical RISs show almost independent performance from the channel model, the performance of practical RISs is significantly dependent on both the characteristics of the channel they operate and the performance of the channel estimation method, depending on their design. Therefore, the channel model and the channel estimation algorithm should be considered together when investigating the performance of practical RISs.

It has been shown in our previous work [18] that it is possible to increase energy-efficiency by using RISs. However, as RISs strictly need CSI to improve the received SNR, we proposed a channel estimation architecture based on GATs in [23] which overperforms least square (LS) estimation. Besides the contributions of [23], this study provides the following main contributions:

C1 By comparing the channel estimation performance of the proposed GAT model and the conventional deep learning (DL) methods, it is shown that the GAT shows a higher performance at low SNR. Moreover, the GAT can remain its performance much more than the conventional DL methods under unobserved channel conditions. It should be noted that the proposed GAT is less time consuming for training due to its short epoch time compared to the conventional DL methods.

C2 In addition to channel estimation, we design time-division duplex (TDD) framework for uplink and downlink signaling of RIS-assisted DtS IoT in order to use channel reciprocity. Due to the motion of satellites, the coherence time is short. Thus, the pilot signaling subframe must

be extremely short duration while the channel estimation method should show high performance with the small number of pilot symbols. In this study, the proposed GAT estimator uses only 16 symbols for the pilot subframe.

C3 The performance of RIS-assisted DtS IoT is investigated for non-ideal RISs with discrete and distinct phase sets as well as ideal RISs when CSI is acquired by the proposed GAT channel estimator. By considering the numerical results, the relation between RIS design and the channel models is discussed.

The rest of this paper is organized as follows. Section II introduces the basic background for GATs and RIS-assisted satellite communications. In Section III, the system model is detailed for RIS-assisted DtS IoT supported by GAT channel estimator. Section IV describes channel estimation procedure from dataset generation to training by giving the related parameters for GAT. In Section V, numerical results under various RIS configurations are discussed. Finally, Section VI dwells on the open issues and concludes the study.

II. PRELIMINARIES

In this section, the fundamentals for each part of the proposed RIS-assisted satellite IoT communication with GATs channel estimator are introduced. First, we present the GAT in detail. Then, RIS-assisted satellite links are discussed. It should be noted that the notation used in this section is given for downlink; however, it can be used for the uplink transmission without loss of generality.

A. Graph Attention Networks

Graph neural networks have been recently proposed as a state-of-the-art solution for data that does not exhibit a grid-like structure while most of the deep learning methods are utilized for the data in the regular domain. GAT, which is one of the graph neural networks, is prominent for inductive learning thanks to its attention mechanism. Inductive learning provides the generalization of a trained network over unobserved graphs. Considering the random nature of the propagation medium, GAT is suitable to be utilized over unobserved channel states.

A GAT consists of graph attention layers (GALs) with P input nodes denoted by $\vartheta = \left\{ \vec{\vartheta}_1, \vec{\vartheta}_2, \ldots, \vec{\vartheta}_P \right\}$, $\vec{\vartheta}_i \in \mathbb{R}^F$. F stands for the number of features in each node. The output set of node features for GAL can be shown by a new set $\vartheta' = \left\{ \vec{\vartheta}'_1, \vec{\vartheta}'_2, \ldots, \vec{\vartheta}'_P \right\}$, $\vec{\vartheta}'_i \in \mathbb{R}^{F'}$. Since the cardinality for the output and input might be different, the number of features is represented by F'. The input properties of each node are transformed to higher-level properties by utilizing a linear transformation described by the weight matrix, $\mathbf{W} \in \mathbb{R}^{F \times F'}$. Then, the attention mechanism, $a : \mathbb{R}^{F'} \times \mathbb{R}^{F'} \rightarrow \mathbb{R}$, is employed to evoke the self-attention on nodes. The attention coefficients are computed as follows:

$$c_{ij} = a \left(\mathbf{W} \vec{\vartheta}_i, \mathbf{W} \vec{\vartheta}_j \right), \quad (1)$$

where c_{ij} denotes the neighborhood between the i-th and j-th nodes in the graph. The attention coefficients reveal how
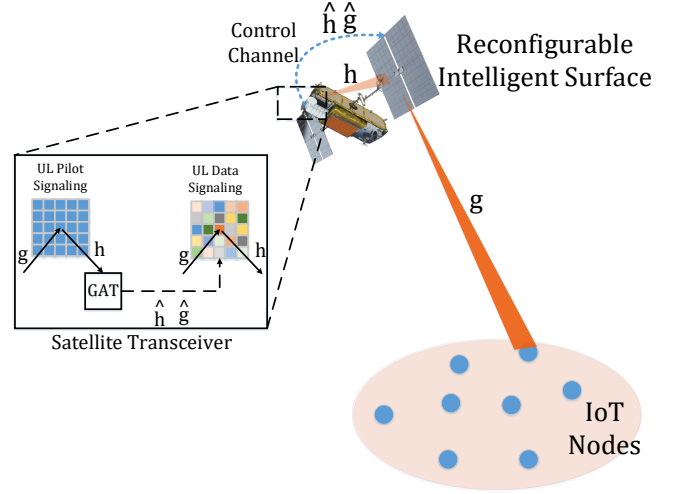

Fig. 2. Direct-to-Satellite IoT communications assisted by RIS with the GAT channel estimator. The estimated channel state information is employed to reconfigure RIS elements.

much the features of the j-th node have an impact on the i-th node. By using a softmax function, the attention coefficients are normalized as given [28]

$$\alpha_{ij} = \text{softmax}_j \left(c_{ij} \right) = \frac{\exp \left(c_{ij} \right)}{\sum_{k \in \mathcal{N}_i} \exp \left(c_{ik} \right)}, \quad (2)$$

where the neighborhood for i-th node is denoted by $\mathcal{N}_i$. The attention mechanism determines the normalized coefficients, α_{ij}, as [24]

$$\alpha_{ij} = \frac{\exp \left(\text{ReLU} \left(\mathbf{a}^\top \left[(\mathbf{XW})_i \| (\mathbf{XW})_j \right] \right) \right)}{\sum_{k \in \mathcal{N}(i)} \exp \left(\text{ReLU} \left(\mathbf{a}^\top \left[(\mathbf{XW})_i \| (\mathbf{XW})_k \right] \right) \right)}, \quad (3)$$

where $\mathbf{X} \in \mathbb{R}^{P \times F}$ and $\mathbf{a} \in \mathbb{R}^{2F'}$ are node features and attention kernel, respectively. The convolution operation is performed over the graph network as follows

$$\mathbf{Z} = \alpha \mathbf{XW} + \mathbf{b}, \quad (4)$$

where $\mathbf{b}$ refers to the trainable bias vector. The inputs of this layer are the node attributes matrix $\mathbf{X} \in \mathbb{R}^{P \times F}$, the edge attributes matrix $\mathbf{E} \in \mathbb{R}^{P \times P \times S}$, and the binary adjacency matrix $\mathbf{A} \in \{0, 1\}^{P \times P}$. Moreover, a pooling layer is employed to generalize graph convolution networks [25]. Besides generalization, the pooling layer enables to decrease the number of representations. As a result, it can be said that the pooling layer avoids the graph neural network to overfit. We employ only global attention pooling layer in the proposed graph neural network. The output of global attention pooling for the input, $\mathbf{X}$, can be given as

$$\mathbf{X}' = \sum_{i=1}^{P} \left(\sigma \left(\mathbf{XW}_1 + \mathbf{b}_1 \right) \odot \left(\mathbf{XW}_2 + \mathbf{b}_2 \right) \right)_i. \quad (5)$$

In (5), σ denotes the sigmoid function and $\odot$ is the broadcast elementwise product.

B. RIS-assisted LEO Satellite Communications

In this section, we introduce a system model of RIS-assisted DtS communications for IoT networks. As known that relays can show higher performance when they become closer to the receiver or the transmitter, RIS is deployed near the satellite antenna as illustrated in Fig. 2. Thus, the system scheme provides a two-fold gain which is maximizing improvement and avoiding extra wireless frounthaul between transmitter and RIS for CSI. It is worth noting that the satellite antenna is aligned with the normal line of the RIS to maximize the normalized radiation pattern [18]. Under this system model, the received signal reflected by RIS, r, can be given as

$$r = \sqrt{P_t \xi} \mathbf{g}^{\mathrm{T}} \mathbf{\Phi} \mathbf{h} x + w, \tag{6}$$

where the transmitted signal with power P_t and additive white Gaussian noise (AWGN) at receiver are shown by x and $w \sim \mathcal{CN}(0, N_0)$, respectively. ξ is the total path loss in RIS-assisted communications, as detailed in [18]. As the transmit antenna is near the RIS, it is worthwhile to employ the near-field beamforming scheme against the attenuation due to atmosphere [18]. $\mathbf{h} = [h_1, h_2, \ldots, h_N]$ and $\mathbf{g} = [g_1, g_2, \ldots, g_N]$ stand for the channel coefficient vectors, where $h_i = \beta_i e^{j\theta_i}$ and $g_i = \rho_i e^{j\nu_i}$. In this study, the amplitude coefficients, β_i and ρ_i, are assumed to follow the Rician distribution with the shape parameter of $K = 10$ to evaluate a slight multipath fading [29, 30]. θ_i and ν_i denote the phase response of the channels regarding the i-th RIS element. Also, $\mathbf{\Phi}$ is the RIS phase shift matrix given as

$$\mathbf{\Phi} = \mathrm{diag}\left\{ A_1 e^{-j\phi_1}, \ldots, A_N e^{-j\phi_N} \right\}, \tag{7}$$

where ϕ_i and A_i denotes the phase and amplitude response of i-th RIS element. It is worth mentioning that RIS is assumed as a lossless device throughout this study; hence, $A_i = A = 1, \forall i$. Besides, ϕ_i is determined through the estimated channel coefficients, $\hat{h}_i$ and $\hat{g}_i$, as follows

$$\phi_i = \hat{\theta}_i + \hat{\nu}_i, \tag{8}$$

where $\hat{\theta}_i$ and $\hat{\nu}_i$ are the phase shift values estimated by the GAT channel estimator.

Then, the instantaneous effective SNR, γ^{eff}, is given as follows

$$\gamma^{\mathrm{eff}} = \frac{P_t \xi \left| \left(\sum_{i=1}^N \beta_i \rho_i e^{j\psi_i} \right) \right|^2}{N_0}, \tag{9}$$

where $\psi_i = \phi_i - \theta_i - \nu_i$ and $\psi_i = 0$ for the ideal channel estimation.

III. DIRECT-TO-SATELLITE IoT COMMUNICATIONS

In this section, LEO satellite-enabled IoT communications system model is introduced. Before detailing the system model, we would describe the motivations behind the proposed system model. In this study, narrow band modulation based physical layer is adopted. This scheme utilizes a signal with a carrier which has very narrow bandwidth. By employing this scheme, it is possible to design low-complex transceivers [31]. Thus, the cost for transceiver part of IoT devices can be
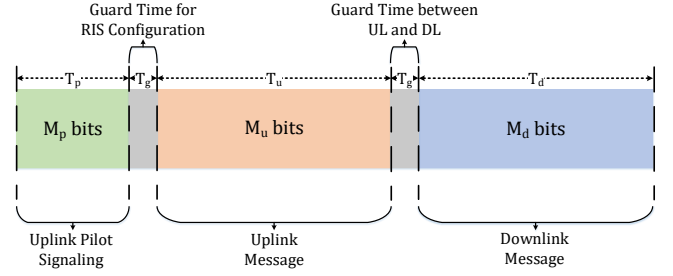

Fig. 3. Each TDD frame consists of uplink pilot signaling, uplink message and downlink message subframes. The frame starts with pilot signaling to estimate channel coefficients regarding to RIS elements.

reduced. Moreover, it should be noted that narrow band modulation can show resistance to noise and interference due to its high power spectral density [32]. Therefore, it is possible to employ ultra-narrow band signals on shared frequency bands. Another appealing feature of ultra-narrow band modulation is that it enables long-range communication link with low-power consumption [33]. As a result, ultra-narrow band modulation techniques can provide to employ low-complex transceiver design in both satellite and IoT devices. Moreover, it can increase battery life by using low power for transmit and reception. However, besides all the appealing features of ultra-narrow band, data rates supported by the ultra-narrow band signals are very low.

Two methods can be proposed to increase the data rate: increasing the modulation degree and/or increasing the bandwidth. Since the required received SNR value raises with increasing the modulation degree, the transmission power should also be increased. This reduces energy-efficiency. Since increasing the bandwidth increases the in-band noise in the receiver, it is evident to increase the transmitted power. More importantly, the equalizer is required in the receiver in order to mitigate multipath fading. To improve energy-efficiency, we have recently proposed RIS-assisted satellite IoT communications in [18]. In this study, we revise the link budget analysis and achieved capacity for RIS-assisted satellite IoT communication under the assumption of the perfect channel state information. [18] shows that RISs can achieve significant improvement in energy-efficiency for both uplink and downlink. Noting that RISs are devices that can process signals at rather than transmitter and receiver, the transceiver complexity can be reduced. RISs can perform equalizer tasks over a communication medium instead of transceivers [10]. Thus, the cost of IoT devices can remain the same while increasing the bandwidth because of no need for an equalizer.

We adopt TDD for uplink and downlink communications to exploit channel reciprocity. By uplink pilot signaling, the CSI is estimated in the satellite by utilizing GATs as detailed later. Each TDD frame includes M_p uplink pilot symbols, M_u uplink message symbols, and M_d downlink message symbols. Furthermore, TDD frame consists of guard intervals for RIS configuration and avoiding interference between uplink and downlink signals. A TDD frame is illustrated in Fig. 3. It is worth noting that the total length of TDD subframe is less than the coherence interval. The M_p-length pilot symbols are

TABLE I
SUMMARY OF THE DATASET PARAMETERS EMPLOYED DURING TRAINING AND TEST.

Parameters	Training	Test
PN Polynomial	$x^4 + x^2 + 1$	$x^4 + x^2 + 1$
Modulation	BPSK	BPSK
# of Samples per SNR	1000	500
SNR (dB)	-30:2:0	-30:2:10
K	10	10
M_p	16	16
N	16, 32, 64	16, 32, 64

selected as a pseudo-noise (PN) sequence generated by the polynomial given by $x^4 + x^2 + 1$. Using PN sequence provides time synchronization between satellite and IoT devices and the detection of the starting point of TDD frame. Additionally, PN sequence might be utilized to identify IoT device by assigning unique sequences for each device.

After channel estimation, RIS elements are configured to maximize the received SNR. Then, the uplink signal can be demodulated without a complex equalizer because RIS can mitigate the random behavior of wireless channels. For downlink communication, the configured RIS is illuminated by the transmitter antenna on the satellite. The reflected signal reaches the IoT device with a high SNR due to the reciprocal channel. In consequence, IoT device can demodulate the reflected signal with low power consumption [18].

This scheme mandates to have an uplink pilot signal for channel estimation before downlink, and therefore sending a message in the downlink depends on the presence of uplink communication. However, when a satellite needs to send a downlink message without waiting for a message from the uplink, the target IoT devices can be evoked by operating RIS in broadcasting mode. Evoked IoT sends uplink pilot sequence for channel estimation.

It is important to note that the proposed scheme is well suited to random time multiple access techniques such as ALOHA and time-slotted ALOHA or time division multiple access (TDMA). However, random frequency multiple access can be supported by providing extra functionalities to the system. For example, a wideband RIS design is required for multiple access based on frequency domain.

IV. CHANNEL ESTIMATION PROCEDURE

This section is devoted to introducing the proposed channel estimation methodology with GATs. As mentioned earlier, the attractive functionality of GATs that allows it to generalize to graphs that have not been completely observed during training [24] makes it a healer for channel estimation in RIS-assisted communications. Unlike the channel estimation methods such as [19, 20] based on switching RIS elements, the proposed GAT channel estimator is able to acquire all channel coefficients regards to RIS elements in a single pilot signaling subframe. Due to motion of LEO satellites, channel coefficients rapidly change. Therefore, accurate channel estimation in LEO satellites requires a generalizable network to

keep estimation performance stable. As mentioned above, it is possible to generalize GATs to unobserved graphs [24].

A. Dataset Generation

The channel coefficients, $\mathbf{h}$ and $\mathbf{g}$, are estimated at the satellite by using uplink pilot signaling. To do this, M_p-length pilot subframes are created by using PN sequence created by the polynomial $x^4 + x^2 + 1$. Assigning different PN sequences to each IoT device allows both identifying the device at the satellite side and keeping synchronization. All meta-atoms are switched on with zero-phase shift, scilicet unitary phase shift matrix. To include a slight multipath effect in the dataset, we select β_i and ρ_i as Rice distributed with the shape parameter $K = 10$. It is worth noting that the GAT channel estimator can remain the estimation performance under different multipath characteristics as shown in [23]. By setting the parameters given above, the dataset has been created. The dataset consists of the input regarding received signal, $\mathbf{X}$, and the adjacency matrix, $\mathbf{A}$, for the graph network including the real and imaginary parts of channel coefficients. $\mathbf{X}$ and $\mathbf{A}$ are expressed as follows

$$\mathbf{X} = [\mathrm{Re}\{\mathbf{y}\}; \mathrm{Im}\{\mathbf{y}\}] \tag{10}$$

$$\mathbf{A} = \begin{bmatrix} 0 & 1 \\ 1 & 0 \end{bmatrix}. \tag{11}$$

$\mathbf{A}$ denotes that a single edge connects two nodes as depicted in Fig. 4. Also, the dataset includes the weight matrix of the edge for the j-th nonzero element of adjacency matrix given as

$$\mathbf{E}_j = \mathbf{s}, \ \mathbf{E} \in \mathbb{C}^{2 \times 2 \times M}. \tag{12}$$

The label vector, $\mathbf{y}$, including the known channel coefficients is generated as

$$\mathbf{y} = [h_1, h_2, \cdots, h_N, g_1, g_2, \cdots, g_N]^{\mathrm{T}}. \tag{13}$$

The training dataset consists of 1000 input samples for each SNR level within -30 dB and 0 dB. The step size for SNR levels is 2 dB. The total number of input samples in the training dataset is 16000 for each N, and SNR values. The training dataset has been divided into two parts: training and validation with the rate of $4 : 1$. Table I summarizes the parameters that are used during the dataset generation.

B. GAT Model and Training

This section details the parameters of the proposed GAT model that is implemented by using Spektral [34]. The model consists of two consecutive GALs. The first and second layers have 128 and 32 output channels, respectively. Each layer employs the ReLU activation function. The size of the input becomes $P = 2$, $F = M$, and $S = M$. Following GALs, a global attention pooling layer is utilized to avoid the model overfitting by decreasing the number of representations. Moreover, it is worth noting that each GAL dropouts fifty-percent of the representations in order to reduce the model complexity as well avoiding overfitting.

Besides dropouts, the network employs L$_2$ regularization. The learning flow through the network is terminated by a
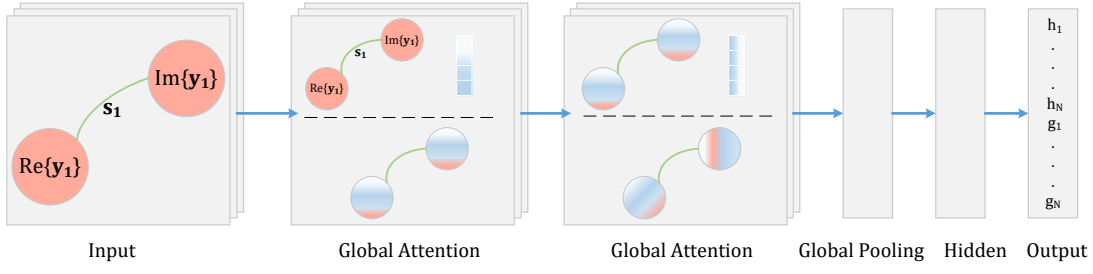
Fig. 4. The illustration for the proposed graph attention network including two consecutive graph attention networks and global attention pooling. The real and imaginary parts of received signal, **y**, are assigned to attributes of two nodes. The edge attributes are set as the pilot symbols, **s**.

TABLE II
THE PARAMETERS AND LAYOUT FOR THE PROPOSED GAT CHANNEL ESTIMATOR.

	Layers	Dimensions
Inputs	**X**	$2 \times M_p$
	A	2×2
	E	$2 \times 2 \times M_p$
Labels	**y**	$4N \times 1$
Graph Attention 1		2×128
Graph Attention 2		2×32
Global Attention Pool		128
Dense		$4N$
Parameters		**Values**
Activation		ReLU
Optimizer		Adam
Loss		MSE
Learning Rate		1e-3
L_2 Regularization		5e-4

hidden layer with $4N$ neurons. In accordance with the nature of the channel estimation problem, the loss function is chosen as mean square error (MSE). To minimize the loss function, ADAM optimizer with a learning rate of 10^{-3} is employed when compiling the network. Although the number of epochs is determined as 20, the early stopping is activated to keep training time short if the loss function does not decrease for 5 epochs. Table II summarizes the GAT parameters and inputs.

V. NUMERICAL RESULTS AND DISCUSSIONS

In this section, the performance of RIS-assisted satellite IoT communications is investigated under GAT channel estimation procedure detailed in the previous section. As [23] denotes that the GAT estimator is able to keep the same estimation performance for the decreasing number of pilot symbols. Therefore, we keep the length of pilot signaling less as much as possible to avoid pilot contamination. In this study, the number of pilot symbols, M_p is selected as 16. Moreover, the GAT estimator is robust to changes in fading statistics, due to attention mechanism [23, 24]. However, in this study, we consider only Rician fading with the shape parameter of $K = 10$ to allow slight non-line-of-sight (NLOS) components in the channel model. The simulation parameters are summarized in the test column of Table I.
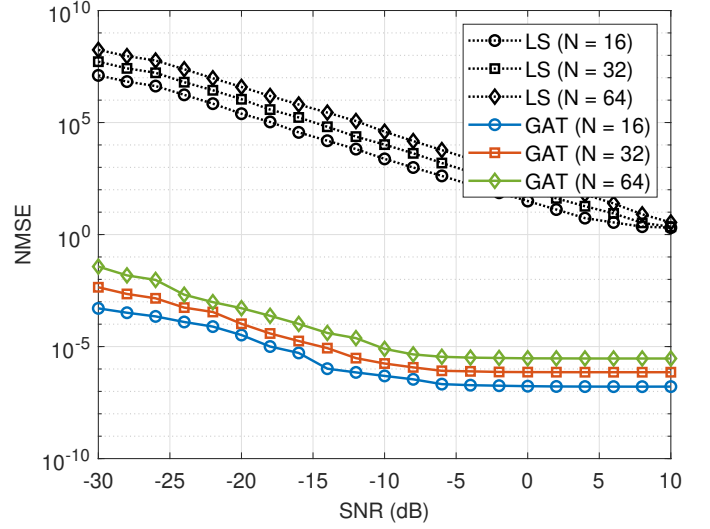

Fig. 5. NMSE performance of the proposed GAT-aided RIS-assisted satellite-to-IoT cascaded channel estimation versus the SNRs, the number of RIS elements, N for $M_p = 16$ and $K = 10$.
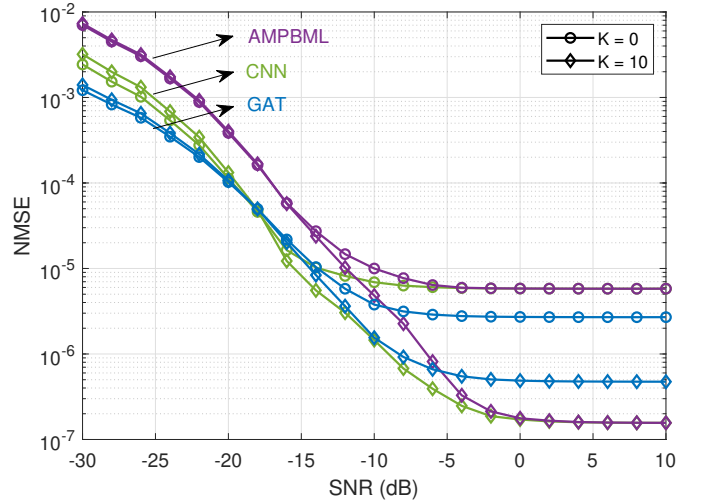

Fig. 6. NMSE performance of the proposed GAT and other DL methods, the number of RIS elements, $N = 16$ for $M_p = 16$ and $K = 0$ and 10. It is observed that the proposed GAT shows a higher performance than the conventional DL methods under changing channel conditions. These results denote the importance of attention mechanism and inductive learning.

Firstly, the channel estimation performances for both **h** and **g** are considered in Fig. 5. The proposed GAT estimator
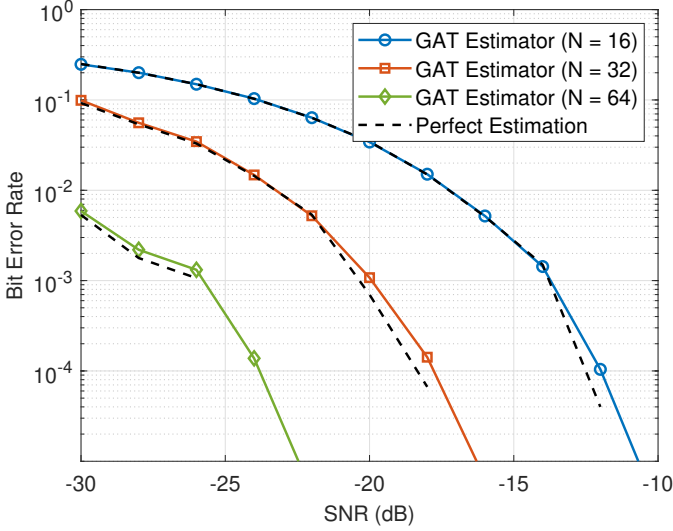
Fig. 7. BER performance of RIS-assisted satellite IoT communications with BPSK signaling under the ideal channel estimation and GAT-based estimation.
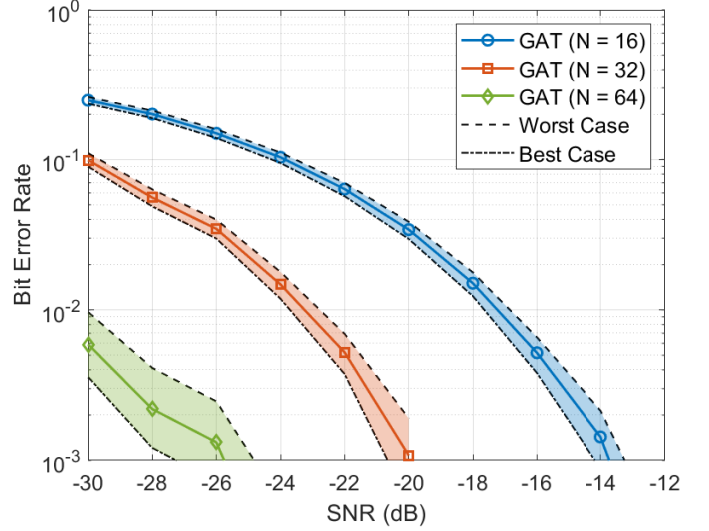

Fig. 8. The confidence interval of BER performance for training procedures. The GATs are trained without any change in the parameters and training sets.

outperforms LS estimation in terms of NMSE. It is seen that both methods require an additional 3 dB SNR when the number of meta-atoms is doubled. But, it should be noted that the required transmit power reduces 3 dB since doubling the number of elements decreases 6 dB the required transmit power [12, 13]. However, the proposed GAT estimator is overperformed compared to LS estimator. Furthermore, even though the training set does not include SNR values between 0 and 10 dB, the NMSE performance does not deteriorate as seen in Fig. 5. The NMSE of GAT converges to 10^{-7} for increasing SNR value. Besides LS, we evaluated conventional DL methods for the same problem. In this paper, we discuss the results of two of the recently proposed conventional DL methods, which have the highest performance, compared with the GAT. AMPBML has been proposed in [35] for beam alignment in mmWave massive MIMO. Another method based on convolutional neural network (CNN) has been proposed in [19] for channel estimation in RIS-assisted mmWave communications. The performance of the models, which have been trained in the case of $K = 10$, is investigated under more challenging conditions by also considering the Rayleigh channel (i.e., $K = 0$) in the test dataset. In Fig. 6, it is shown that the proposed GAT overperforms compared to the conventional methods at low SNR. Although GAT performs slightly lower than conventional methods at high SNR, it maintains its performance much better than the conventional DL methods in changing channel conditions. Owing to the GATs' inductive learning ability over unobserved cases, GAT outperforms the aforementioned machine learning methods when the test data contains different channel conditions than the training dataset. These results reveal how important the attention mechanism is in the cases unobserved during training. Further, more detailed studies are needed on how the conventional methods perform under changing conditions due to a lack of inductive learning capability. As stated above, inductive learning due to the attention mechanism in GATs can allow the network to generalize over unobserved graphs

which can mean unobserved channel conditions in this study. It is worth noting that training complexity is another important factor besides performance in DL methods. From this point of view, it is an important advantage to train the proposed GAT model in a shorter time compared to other models. For example, AMPBML and CNN each require 1.8 and 3 times the epoch duration of GAT, respectively. In brief, the proposed GAT both shows a higher performance with increased robustness under changing conditions and has less computational complexity.

Next, the error rate performance of the proposed RIS-assisted DtS IoT system is investigated by considering the channel estimation error resulting from GAT estimator. The channel estimation and then BER analysis are performed for the number of RIS elements of 16, 32, 64. In this case, the RIS is assumed as continuous phase. The simulation results under both the perfect estimation and GAT estimation are given in Fig. 7. It is observed that BER performance in the case of GAT estimator is almost the same with the perfect estimation at low SNR region. As the SNR value increases, there is a very slight degradation in the error performance due to the non-perfect estimation of the GAT. Moreover, Fig. 8 denotes the confidence intervals for trained GAT estimators. In each training phase, the model parameters and training data are kept as the same. However, random initialization and randomness in the optimizer give rise to different trained models with distinct weight matrices. Intuitively, the best case is the almost same as the BER results in case of the perfect estimation. But, the increasing number of RIS elements makes the confidence interval larger by resulting the worst channel estimation error.

Although RISs can be theoretically considered as continuous phase systems, this assumption is not practically feasible due to hardware limitations. Therefore, we consider discrete-phase RISs with GAT channel estimation. Error rate performance is investigated up to quantized 3-bits RISs with the variable number of elements. First, we assume a basic RIS design which enable phase shifts, ϕ_n, in $[-\pi, \pi)$. The step
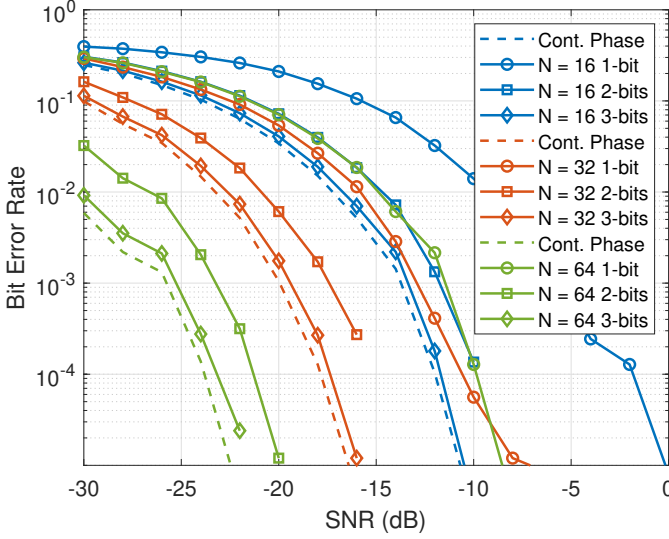
Fig. 9. BER performance of discrete phase RIS-assisted satellite IoT communications with BPSK signaling. Increasing the number of quantization levels proportionally improves the error rate performance of the system.

Fig. 10. The illustration for the phase sets on the unit circle.

size in phase shift set supported by RIS is determined by the number of quantization levels as $\frac{2\pi}{2^{N_{\text{bit}}}}$, where N_{bit} stands for the number of bits. It can be heuristically said that the system performance improves if the number of distinct discrete phase shifts that RIS can provide increases, or in other words, converges to the continuous phase case. Fig. 9 gives the BER results for the quantization levels of 2, 4, and 8. The simulation results denote that increase in the number of quantization levels for phase shifts reduce the error probability. As seen in Fig. 9, 3-bit RIS designs almost approach the error probabilities that the optimum design can achieve. 1-bit designs can only show the same BER performance at higher SNR values compared to 2-bit designs. In other words, 2-bit designs are much more energy-efficient. In addition, considering the cost of RISs that support more than 3-bit quantization levels, it is considered feasible to use 3-bit designs for energy-efficient satellite IoT communication systems.

The phase shifts might not be uniformly distributed in $[-\pi, \pi)$ because of the limitations in intelligent metasurface designs. For example, the phase shift span is proportional to the square-root of the ratio between the effective capacitance and the effective inductance [36]. Because the varactor diode reaches the saturation level (i.e., constant capacitance value) although the control voltage increases, all phase shift values may not be supported by the intelligent surface. For instance, the surface in [37] is able to shift the phase of an incident wave by up to 250 degrees. Hence, we investigate the error rate performance versus the different phase shift sets, namely different RIS designs. We evaluate three sets: Set 1 has been already introduced above. Set 2 and Set 3 only consist of the left-hand side and right-hand side of the phase circle, respectively. The phase shift sets are summarized in Table III and illustrated in Fig. 10. Besides, the discrete phase shifts are employed in this analysis. The phase shift, ϕ_n, is determined as the closest phase value in the set to the phase of the channel
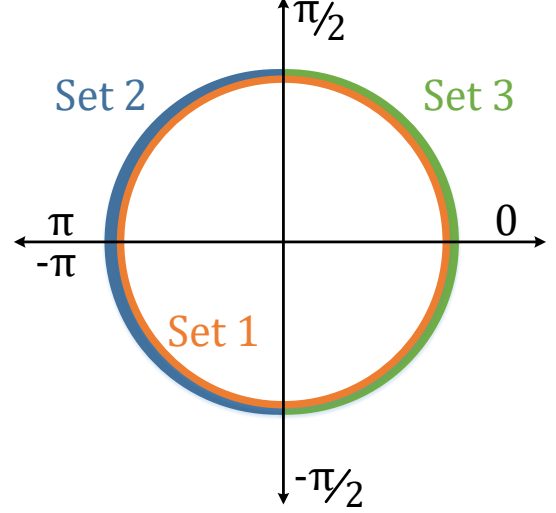
coefficient estimated by GAT as follows:

$$\phi_n = S\{\phi_k : k = \underset{s}{\operatorname{argmin}}(|\phi_s - \angle(\hat{h}_n \hat{g}_n)|)\}, \; s = 1, \cdots, 2^{N_{bit}},$$
(14)

where S is the phase shift set including discrete phase shifts, ϕ_s. $\angle(\cdot)$ stands for the angle operator. Additionally, h_n and g_n denote the estimated channel coefficients regarding the n-th elements of RIS. Fig. 11 denotes the BER performance of RIS-assisted satellite IoT system for the different phase shift sets with 2- and 3-bits. Set 1 and Set 2 show almost similar BER; however, Set 1 results in slightly better error performance. Moreover, BER performance improves when the quantization level increases in the first two sets, while increasing the number of bits in Set 3 surprisingly worsens the performance. To explain this, it is necessary to look closely at the channel model. Fig. 12(a) and Fig. 12(b) show the phase histogram of the actual cascaded channel and the phase histogram of the estimated channel coefficients, respectively.

As can be seen, the phase of the cascaded channel is concentrated around $-\pi$ and π. Likewise, since the channel estimation performance is high, the information about the estimated channels is parallel to the actual channel. These histograms show why Set 1 and Set 2 both performed similarly and have higher performance compared to Set 3. Since the working principle of RIS is to make the SNR maximum by eliminating the phase information of the cascaded channel, RIS must support phase shifts in a way that eliminates the phases of the cascaded channel. Set 1 and Set 2 support the phase shifts of the channels to omit the phases concentrated around $-\pi$ and π. However, since Set 3 consists of phase shifts between $-\pi/2$ and $\pi/2$, it cannot completely exclude actual phases around $\mp\pi$. In addition, increasing the quantization level also allows correcting the actual phases different from $\mp\pi$ in Set 1 and Set 2. The increase in the number of levels enables the generation of new phase values between $-\pi/2$ and $\pi/2$ in Set 3 and creates phase shifts more far away from

TABLE III
THE PHASE SETS WITH DIFFERENT SPANS BETWEEN $-\pi$ AND π.

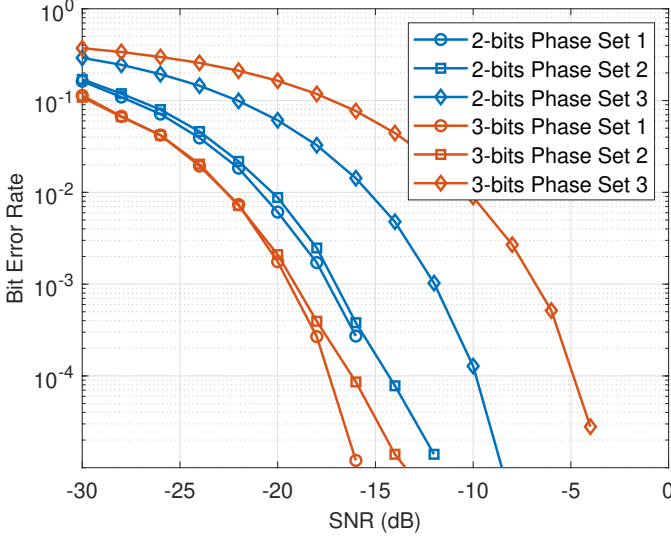| Phase Set	Phase Interval	Step Size
Set 1	$[-\pi, \pi)$	$\frac{2\pi}{2^{N_{bit}}}$
Set 2	$(-\pi, -\frac{\pi}{2}] \cup [\frac{\pi}{2}, \pi)$	$\frac{\pi}{2^{N_{bit}}}$
Set 3	$[-\frac{\pi}{2}, \frac{\pi}{2}]$	$\frac{\pi}{2^{N_{bit}}}$

Fig. 11. BER performance of discrete phase 32-elements RIS-assisted satellite IoT communications regarding different phase sets.
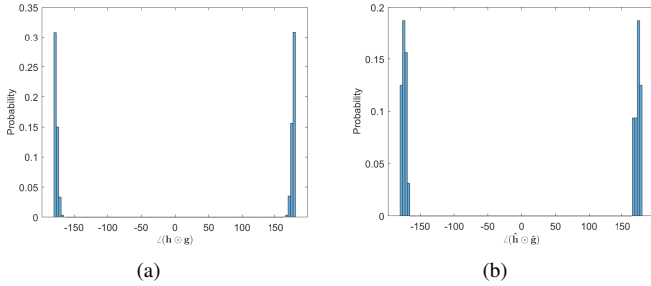

Fig. 12. The histogram for the phase of (a) actual, and (b) estimated channel coefficients.

$\mp\pi$. Therefore, the phase information cannot be adequately corrected.

VI. RESEARCH DIRECTIONS AND CONCLUDING REMARKS

In this study, GAT based channel estimation is presented for RIS-assisted communications and it is shown that high performance is achieved. The proposed channel estimation method based on GAT is able to learn inductively; therefore, it can provide high performance under changing conditions that are not included in the training phase.

To improve DtS IoT systems, RIS with GAT is integrated to the system architecture. By doing so, it is demonstrated that the error probability is achieved at lower SNR compared to conventional methods. BER performance under various RIS configurations including discrete and piecewise phase sets is numerically investigated. It is shown that a 2-bit resolution

can perform as well as ideal RISs that can produce almost continuous phase shift. In addition, the simulation results show that the channel model is an important design parameter in RIS design. This study provides a comprehensive investigation on GAT-based channel estimation and performance analysis on RIS-assisted DtSs; however, the impact of Doppler shift to GAT performance due to the motion of LEO satellites requires more investigation. Moreover, RIS fabrication and deployment on satellites requires consideration of space conditions and SWaP constraints, so it should be the subject of interdisciplinary research.

REFERENCES

[1] A. Nassar and Y. Yilmaz, "Deep reinforcement learning for adaptive network slicing in 5G for intelligent vehicular systems and smart cities," *IEEE Internet Things J.*, vol. 9, no. 1, pp. 222–235, 2022.

[2] T. Sanislav, G. D. Mois, S. Zeadally, and S. C. Folea, "Energy harvesting techniques for internet of things (IoT)," *IEEE Access*, vol. 9, pp. 39 530–39 549, 2021.

[3] G. A. Akpakwu, B. J. Silva, G. P. Hancke, and A. M. Abu-Mahfouz, "A survey on 5G networks for the Internet of Things: Communication technologies and challenges," *IEEE Access*, vol. 6, pp. 3619–3647, 2017.

[4] J. A. Fraire, S. Céspedes, and N. Accettura, "Direct-to-satellite IoT- a survey of the state of the art and future research perspectives," in *International Conference on Ad-Hoc Networks and Wireless*. Springer, 2019, pp. 241–258.

[5] J. A. Fraire, S. Henn, F. Dovis, R. Garello, and G. Taricco, "Sparse satellite constellation design for LoRa-based direct-to-satellite internet of things," in *IEEE Global Communications Conference*, 2020, pp. 1–6.

[6] R. Barbau, V. Deslandes, G. Jakllari, J. Tronc, J.-F. Chouteau, and A.-L. Beylot, "NB-IoT over GEO satellite: performance analysis," in *Advanced Satellite Multimedia Systems Conference and the Signal Processing for Space Communications Workshop*, 2020, pp. 1–8.

[7] C. A. Hofmann and A. Knopp, "Direct access to GEO satellites: An Internet of Remote Things technology," in *IEEE 5G World Forum*, 2019, pp. 578–583.

[8] S. Cluzel, L. Franck, J. Radzik, S. Cazalens, M. Dervin, C. Baudoin, and D. Dragomirescu, "3GPP NB-IoT coverage extension using LEO satellites," in *IEEE Vehicular Technology Conference*, 2018, pp. 1–5.

[9] Z. Qu, G. Zhang, H. Cao, and J. Xie, "LEO satellite constellation for Internet of Things," *IEEE Access*, vol. 5, pp. 18 391–18 401, 2017.

[10] E. Basar, M. Di Renzo, J. De Rosny, M. Debbah, M.-S. Alouini, and R. Zhang, "Wireless communications through reconfigurable intelligent surfaces," *IEEE Access*, vol. 7, pp. 116 753–116 773, 2019.

[11] Q. Wu and R. Zhang, "Towards smart and reconfigurable environment: Intelligent reflecting surface aided wireless network," *IEEE Commun. Mag.*, vol. 58, no. 1, pp. 106–112, 2019.

[12] K. Tekbıyık, G. K. Kurt, A. R. Ekti, and H. Yanikomeroglu, "Reconfigurable intelligent surfaces in action for non-terrestrial networks," *arXiv preprint arXiv:2012.00968*, 2020.

[13] K. Tekbıyık, G. K. Kurt, A. R. Ekti, A. Görçin, and H. Yanikomeroglu, "Reconfigurable intelligent surface empowered terahertz communication for LEO satellite networks," *arXiv preprint arXiv:2007.04281*, 2020.

[14] L. Dai, B. Wang, M. Wang, X. Yang, J. Tan, S. Bi, S. Xu, F. Yang, Z. Chen, M. Di Renzo *et al.*, "Reconfigurable intelligent surface-based wireless communications: Antenna design, prototyping, and experimental results," *IEEE Access*, vol. 8, pp. 45 913–45 923, 2020.

[15] W. Tang, J. Y. Dai, M. Z. Chen, K.-K. Wong, X. Li, X. Zhao, S. Jin, Q. Cheng, and T. J. Cui, "MIMO transmission through reconfigurable intelligent surface: System design, analysis, and implementation," *IEEE J. Sel. Areas Commun.*, vol. 38, no. 11, pp. 2683–2699, 2020.

[16] J. Hu, H. Zhang, B. Di, L. Li, K. Bian, L. Song, Y. Li, Z. Han, and H. V. Poor, "Reconfigurable intelligent surface based RF sensing: Design, optimization, and implementation," *IEEE J. Sel. Areas Commun.*, vol. 38, no. 11, pp. 2700–2716, 2020.

[17] C. Huang, A. Zappone, G. C. Alexandropoulos, M. Debbah, and C. Yuen, "Reconfigurable intelligent surfaces for energy efficiency in wireless communication," *IEEE Trans. on Wirel. Commun.*, vol. 18, no. 8, pp. 4157–4170, 2019.

[18] K. Tekbıyık, G. K. Kurt, and H. Yanikomeroglu, "Energy-efficient RIS-assisted satellites for IoT networks," *IEEE Internet Things J. Early Access*, pp. 1–10, 2021.

[19] A. M. Elbir, A. Papazafeiropoulos, P. Kourtessis, and S. Chatzinotas, "Deep channel learning for large intelligent surfaces aided mm-Wave massive MIMO systems," *IEEE Wireless Commun. Lett.*, vol. 9, no. 9, pp. 1447–1451, 2020.

[20] D. Mishra and H. Johansson, "Channel estimation and low-complexity beamforming design for passive intelligent surface assisted MISO wireless energy transfer," in *Proc. IEEE ICASSP*, 2019, pp. 4659–4663.

[21] G. E. Corazza and F. Vatalaro, "A statistical model for land mobile satellite channels and its application to nongeostationary orbit systems," *IEEE Trans. Veh. Technol.*, vol. 43, no. 3, pp. 738–742, 1994.

[22] A. Taha, M. Alrabeiah, and A. Alkhateeb, "Enabling large intelligent surfaces with compressive sensing and deep learning," *IEEE Access*, vol. 9, pp. 44 304–44 321, 2021.

[23] K. Tekbıyık, G. K. Kurt, C. Huang, A. R. Ekti, and H. Yanikomeroglu, "Channel estimation for full-duplex RIS-assisted HAPS backhauling with graph attention networks," in *IEEE International Conference on Communications*, 2021, pp. 1–6.

[24] P. Veličković, G. Cucurull, A. Casanova, A. Romero, P. Lio, and Y. Bengio, "Graph attention networks," in *The International Conference on Learning Representations*, 2018, pp. 1–12.

[25] J. Lee, I. Lee, and J. Kang, "Self-attention graph pooling," in *Proceedings of the 36th International Conference on Machine Learning*, vol. 97. PMLR, 09–15 Jun 2019, pp. 3734–3743.

[26] E. Basar, "Reconfigurable intelligent surfaces for Doppler effect and multipath fading mitigation," *arXiv preprint arXiv:1912.04080*, 2019.

[27] I. Yildirim, A. Uyrus, and E. Basar, "Modeling and analysis of reconfigurable intelligent surfaces for indoor and outdoor applications in future wireless networks," *IEEE Trans. on Commun.*, vol. 69, no. 2, pp. 1290–1301, 2021.

[28] D. Bahdanau, K. Cho, and Y. Bengio, "Neural machine translation by jointly learning to align and translate," *arXiv preprint arXiv:1409.0473*, 2014.

[29] N. Letzepis and A. J. Grant, "Capacity of the multiple spot beam satellite channel with Rician fading," *IEEE Trans. Inf. Theory*, vol. 54, no. 11, pp. 5210–5222, 2008.

[30] L. You, K.-X. Li, J. Wang, X. Gao, X.-G. Xia, and B. Ottersten, "Massive MIMO transmission for LEO satellite communications," *IEEE J. Sel. Areas Commun.*, vol. 38, no. 8, pp. 1851–1865, 2020.

[31] M. Anteur, V. Deslandes, N. Thomas, and A.-L. Beylot, "Ultra narrow band technique for low power wide area communications," in *IEEE Global Communications Conference*, 2015, pp. 1–6.

[32] T. Lassen, "Long-range RF communication: Why narrowband is the de facto standard," https://www.ti.com/lit/wp/swry006/swry006.pdf, 2014, (Accessed on 14/12/2021).

[33] X. Xiong, K. Zheng, R. Xu, W. Xiang, and P. Chatzimisios, "Low power wide area machine-to-machine networks: key techniques and prototype," *IEEE Commun. Mag.*, vol. 53, no. 9, pp. 64–71, 2015.

[34] D. Grattarola and C. Alippi, "Graph neural networks in Tensorflow and Keras with Spektral," *IEEE Comput. Intell. Mag.*, vol. 16, no. 1, pp. 99–106.

[35] W. Ma, C. Qi, and G. Y. Li, "Machine learning for beam alignment in millimeter wave massive MIMO," *IEEE Wireless Commun. Lett.*, vol. 9, no. 6, pp. 875–878, 2020.

[36] F. Liu, O. Tsilipakos, A. Pitilakis, A. C. Tasolamprou, M. S. Mirmoosa, N. V. Kantartzis, D.-H. Kwon, J. Georgiou, K. Kossifos, M. A. Antoniades *et al.*, "Intelligent metasurfaces with continuously tunable local surface impedance for multiple reconfigurable functions," *Physical Review Applied*, vol. 11, no. 4, p. 044024, 2019.

[37] W. Tang, X. Li, J. Y. Dai, S. Jin, Y. Zeng, Q. Cheng, and T. J. Cui, "Wireless communications with programmable metasurface: Transceiver design and experimental results," *China Communications*, vol. 16, no. 5, pp. 46–61, 2019.